Nanoscale

Accepted Manuscript

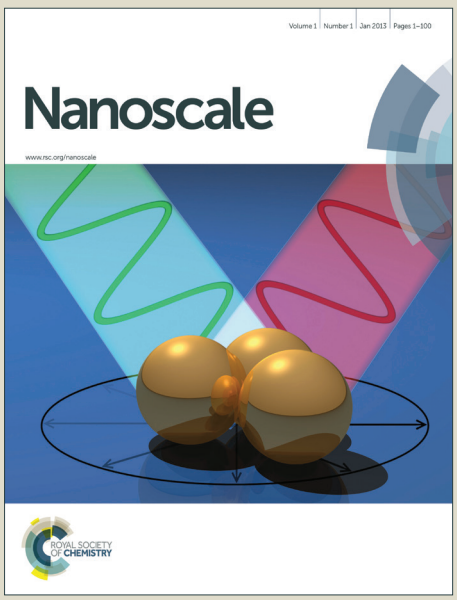

This is an *Accepted Manuscript*, which has been through the Royal Society of Chemistry peer review process and has been accepted for publication.

Accepted Manuscripts are published online shortly after acceptance, before technical editing, formatting and proof reading. Using this free service, authors can make their results available to the community, in citable form, before we publish the edited article. We will replace this *Accepted Manuscript* with the edited and formatted *Advance Article* as soon as it is available.

You can find more information about *Accepted Manuscripts* in the Information for Authors.

Please note that technical editing may introduce minor changes to the text and/or graphics, which may alter content. The journal's standard Terms & Conditions and the Ethical guidelines still apply. In no event shall the Royal Society of Chemistry be held responsible for any errors or omissions in this *Accepted Manuscript* or any consequences arising from the use of any information it contains.

ROYAL SOCIETY OF CHEMISTRY

www.rsc.org/nanoscale

Self-ordering of small-diameter metal nanoparticles by dewetting on hexagonal mesh templates

Eric R. Meshot[1,2], Zhouzhou Zhao[1],Wei Lu[1], and A. John Hart[1,3]*

[1] Department of Mechanical Engineering, University of Michigan, 2350 Hayward St., Ann Arbor, MI 48109, USA.

[2] Physical and Life Sciences Directorate, Lawrence Livermore National Laboratory, 7000 East Avenue, Livermore, CA 94551, USA.

[3] Mechanosynthesis Group, Department of Mechanical Engineering, Massachusetts Institute of Technology, Cambridge, MA 02139, USA.

*E-mail: ajhart@mit.edu

Keywords

Nanoparticle, catalyst, order, template, dewetting

Abstract

Arrays of small-diameter nanoparticles with high spatial order and controlled spacing are useful for catalysis, photonic devices, magnetic recording, synthesis of nanowires and nanotubes, and many other applications. We show that self-ordered metal nanoparticle arrays can be formed by dewetting of thin films on hexagonal mesh substrates made of anodic aluminum oxide (AAO). We investigated the particle morphology and dynamics of dewetting using a combination of atomic force microscopy (AFM), grazing-incidence small-angle X-ray scattering (GISAXS), and numerical simulations. The metal film dewets onto the interstitial sites (*i.e.*, the node points) between pores on the top surface of the AAO; this is driven by surface tension about the edges of the holes in the film, which are self-patterned by the geometry of the template. Templated metal particles were more monodisperse and had higher local order than those formed by the same process on flat, nonporous alumina. The degree of order depends on the initial film thickness, and for the optimal thickness tested (nominally 2 nm), we achieved uniform coverage and high order of the particles, comparable to that of the AAO template itself. Computational modeling of dewetting on templates with various pore order and size showed that the order of AAO pores is primarily influential in determining particle position and spacing, while the variance in pore size is less impactful.

Nanoscale Accepted Manuscript

Our study demonstrates that high local hexagonal order is achievable from facile single-step dewetting. Potential uses of these ordered nanoparticle arrays on porous materials include plasmonics and energy storage.

Introduction

Fabricating substrate-supported arrays of metal nanoparticles is widely important for catalysis, photonic devices, magnetic recording, synthesis of nanowires and nanotubes, and other applications. Independent control of the size, spacing, and order of the particles is crucial to enable engineering of properties that rely both on particle dimensions and organization. Various methods to produce nanoparticle arrays have both strengths and limitations. Top-down methods[1, 2, 3, 4-7] are frequently limited by the wavelength of optical lithography, or require use of electron beam lithography, which is relatively costly and low throughput. Bottom-up (self-directed) processes, such as by the use of capillary forces or block copolymers to assist assembly of particles[8] are effective yet often rely on pre-formed nanoparticles or micelles, which adds additional complexity and challenges to the process. Additionally, the presence of the polymer can contaminate or alter the performance or functionality of the particle array.

Dewetting of metal thin films into islands is an alternative, facile, and self-directed route for making particle arrays. Dewetting of pre-patterned thin films can be induced by ion[9] or laser[10] beams as well as by thermal annealing, which is often more accessible compared to techniques requiring high-energy sources. Thermal stress drives solid-state dewetting through surface diffusion of metal atoms at temperatures well below the melting point of the metal,[11] which allows restructuring of the film into islands in order to minimize the energy of the system. However, this process is governed by surface tension that originates from random formation of grain boundaries and holes in the film,[12] so it is challenging to control resultant particle size and spacing.

Researchers have patterned defects or other topographical features on host substrates to control the migration of metal atoms during film dewetting and thus achieve deterministically ordered structures. For example, thin metal films deposited on a substrate with sub-micrometer pits or trenches, preferentially dewet and form particles at the bottom of the pits.[13-16] Giermann and Thompson[14] explain that grooving of the film at the sharp edges of topographical features leads to pinching off of the film as atoms migrate

Nanoscale Accepted Manuscript

away from these highly strained regions. Further studies showed that depending on film thickness and processing conditions, dewetting could be programmed to produce one or several particles per pit.[13, 17] Recent studies combined dewetting with other mechanisms to fabricate arrays. For instance, Ye and Thompson[18] exploited the crystal orientation of single-crystal Ni films. They showed that arrays of different complex shapes can be generated from the same lithographic pattern, depending on the film's crystal orientation. Farzinpour, *et al*.[19] deposited metal films on top of sacrificial antimony patterns and then generated regular arrays of ~100 nm particles by sublimating the antimony away during heating. However, to our knowledge, templated dewetting has not been studied at the ~10-nm scale due to the inherent challenges of patterning surface topographies with small feature size.

Here, we study the self-ordering of metal nanoparticle arrays by dewetting of thin films on hexagonal mesh substrates made of nanoporous anodic aluminum oxide (AAO). We deposited metal films on the top surface of AAO substrates and found that upon thermal annealing, the metal film dewets onto the interstitial sites (*i.e*., the node points) between pores on the top surface of the AAO. This is driven by surface tension around the edges of holes in the film, which are self-patterned by the geometry of the template. Using atomic force microscopy (AFM), grazing-incidence small-angle X-ray scattering (GISAXS), and numerical simulations, we show that metal particles formed on AAO are more monodisperse and have higher local hexagonal order than on flat control substrates. The organization of the templated particles is related to the initial film thickness and the relative order of the AAO pores.

Nanoscale Accepted Manuscript

Results and discussion

We focused our study on dewetting of Fe because it is has broad applicability for magnetic devices, catalysis, and growth of carbon nanostructures; however, our approach is generally valid for metals and other materials that can be deposited in a line-of-sight configuration. As illustrated in Figure 1, Fe metal films are sputtered on the top surface of the AAO substrate and thus are self-patterned by the hexagonally arranged pores. Coating of sputtered thin films is uniform in thickness up to wafer scale areas and yields topography with nanoscale roughness, which is pronounced by the inherent roughness and porous structure of the AAO. Thermal annealing is still required to induce coarsening and fully form particles, which we performed at 775 °C in H_2/He for 10 minutes (see Supplementary Information for details).

During heating, holes in the self-patterned film grow during annealing as metal atoms flow from the highly strained (energetically unfavorable) edges of the holes to the node points on the surface of the AAO. Dewetting occurs upon heating due to capillary instabilities in the film, and surface tension arising at holes in the film drives the diffusion of atoms. This may occur at temperatures as low as 20% of the metal's bulk melting temperature, yet the thermal energy is enough to both induce a compressive stress in the film (due to thermal mismatch between film and substrate) and increase the mobility of metal atoms during surface diffusion, both of which drive film dewetting. Our previous *in situ* GISAXS studies[20] of Fe films (nominally 1 nm) for carbon nanotube (CNT) growth on flat Al_2O_3 demonstrated that dewetting occurs at 550 °C (36% of Fe melting point) and can be rapid (< 10 sec) when heating at 10 °C sec^{-1} in H_2/He. The Fe particles are stable in their size and spacing on the substrate for several minutes thereafter. We also note that the native FeO_x thin film reduces to Fe upon heating, which we found to be critically important for dewetting.

Here, we performed experiments with different Fe thickness deposited on AAO and examined the surface topography before and after by AFM imaging. Local AFM traces of select areas on bare AAO and 2 nm Fe on AAO (*i.e.*, to with and without particles) compare relative height in Figure 2 show the presence of small particles at the node points after deposition and annealing. We conclude that the particle diameter is <20 nm and that the Fe is restricted to the top surface of the AAO. To show that most if not all of the Fe is confined to the top surface, we grew a vertically aligned CNT forest from the particle

Nanoscale Accepted Manuscript

array. Cross-sectional SEM reveals a clean CNT/AAO interface, with no CNTs originating from the AAO pores (Figure S1).

We observe that the initial Fe thickness has a strong influence on the particle order after dewetting on AAO, which is demonstrated in Figure 3 by AFM images and corresponding FFT patterns. FFT analysis of particles formed on AAO from sub-5-nm films exhibit order, evidenced by the pronounced rings characteristic of small variance in particle spacing. The case with 2 nm initial Fe thickness shows markedly better coverage compared to 1 nm with similarly high order according to their respective FFT; however, if the initial film is too thick, the template does not influence order. In comparison, metal films on flat Al_2O_3 dewet according to the random roughness of the underlayer, and thus, the particles are polydisperse in size and spacing, which is evidenced by the diffuse FFT pattern (Figure 3e). A 5 nm film yielded a highly polydisperse particle population lacking order. This suggests that there is a threshold for film thickness, likely due to the fact that it is not energetically favorable for a large particle to be confined to the limited area of a node point on the AAO's surface. We estimate that when the volume of a 5 nm film is divided evenly according to the accessible node density on the AAO support (18 nm, 49 nm spacing from AFM analysis in Figure S2), the average particle diameter is larger than 40 nm, which exceeds the lateral dimension of the available surface of a node.

We also sought to quantify the influence of the AAO template on the Fe particle size. However, this is challenging to do with AFM images due to the presence of the pores and long-range roughness in the surface of AAO. As a result, we employed GISAXS as a complementary technique, which is nondestructive and probes nanoscale surface structure over a large area (>10 mm^2).[21] For our substrates, two characteristic coherent scattering features are present for $0.1 < q < 1$ nm^{-1}: a low-q peak corresponding to the particle-particle spacing, and a high-q peak related to the form factor (size, shape) of the particle. As shown in Figure 3f, bare AAO has a sharp scattering peak at $q = 0.2$ nm^{-1} arising from the interpore spacing ($2\pi/q = 31$ nm), which corroborates the FFT of the corresponding AFM image in Figure 3d. There is nearly no high-q scattering because the top surface of the AAO exhibits no well-defined structures (*i.e.*, random roughness). There is a peak present at a similar q value ~0.2 nm^{-1} for templated particles due to pore spacing because the pores remain exposed for X-rays to scatter from them as long as the initial metal film thickness is small. However, a form-factor peak emerges at $q = 0.4$ nm^{-1} in this

Nanoscale Accepted Manuscript

case due to the presence of well-defined particles on the surface ($2\pi/q$ = 16 nm). This peak is significantly narrower than the corresponding peak for Fe on flat Al_2O_3 at q = 0.7 nm^{-1} (full width at half maximum is 0.07 nm^{-1} versus 0.15 nm^{-1}, respectively), which indicates that particles formed on AAO templates are more monodisperse than those on flat supports.

We quantify the particle order by finding the maximum value of the following expression:

$$Q = \frac{1}{3N}\sum_{i=1}^{N}[\cos\frac{4\pi x_i}{\sqrt{3}\lambda_0} + \cos\frac{4\pi}{\sqrt{3}\lambda_0}(-\frac{x_i}{2} + \frac{\sqrt{3}y_i}{2}) + \cos\frac{4\pi}{\sqrt{3}\lambda_0}(-\frac{x_i}{2} - \frac{\sqrt{3}y_i}{2})] \quad (1)$$

This formulation has been used for highly ordered atomic surface structures.[22] The order parameter Q_{max} is 0 for entirely disordered (random) and 1 for perfectly hexagonally ordered particles. *N* is the total number of particles in the image, λ_0 is the particle spacing, and (x_i, y_i) are the coordinates of each particle. We maximize Q by scanning the following two variables: the spacing λ_0 (from 0.5 to 1.5) and the orientation θ (from 0 to 60°) of the coordinate system (expressed in terms of x_i, y_i). We use a custom MATLAB script to identify the location of particles by scanning for local maxima in both AFM and simulated images.

It is also important to consider that the AAO lacks long-range order and thus the size of the area of analysis influences the calculated order. For large scan sizes, particle arrays on both AAO mesh substrates and flat Al_2O_3 substrates show similarly low order, even though the arrangements of particles seen in AFM images are different. In Figure 4, we quantify the order of particles formed on AAO versus flat substrates, and we show that Fe particles in both cases show higher order when a smaller area is investigated. However, in comparing these two substrates across AFM scan sizes, we observed a 2-fold difference in the order parameter value (0.34 versus 0.18 for templated and flat cases, respectively) when analyzing from AFM image segments smaller than 350 nm, which by inspection corresponds with the approximate domain size of the AAO used in this study. This highlights two important points: the hexagonal mesh template indeed prescribes the formation of ordered arrays by directing dewetting; and the long-range order of the nanoparticle array is inherently limited by the finite grain size and limited long-range order of the AAO template. Although AAO substrates have been reported with larger pores (~50

Nanoscale Accepted Manuscript

nm) having quasi-hexagonal order across several hundred nanometers,[23] such substrates are not widely available to our knowledge.

To complement our experimental approach and explore the design space of AAO-templated dewetting, we also performed computational modeling. We adopted an energetic framework used previously to study dewetting of nanoscale polymeric and metallic films.[24] This approach considered a liquid thin film on a substrate surface as a representative system, where the free energy of the system comprises the surface energy of the film and the van der Waals (VDW) interaction between the metallic film and the substrate. Although the precise physical state of nanoscale metal catalysts is controversial, the framework sufficiently describes the flow of high-mobility metal atoms during dewetting at elevated temperatures (*i.e.*, by surface diffusion), and importantly, the equilibrium state of the final particle arrays is the same regardless of our assumption of the film's physical state. The expression for the free energy *G* is

$$G = \iint [\frac{\gamma}{2}(\nabla h)^2 + V(h)]dA \quad , \qquad (2)$$

where *h* denotes the height (thickness) of the thin film, and the area integration extends over the substrate surface. The first term accounts for the surface energy, which is related to the surface tension of the film (γ). The second term represents the van der Waals interaction, where

$$V(h) = B/h^8 - A/12\pi h^2 \quad . \qquad (3)$$

Here, *A* is the Hamaker constant and *B* is a constant accounting for the strength of short-range repulsion. We normalized the spatial dimension in Eq. 2 by the initial film thickness h_0, and thus, *A* and *B* can be expressed by the dimensionless parameters $A_0 = A/(\gamma {h_0}^2)$ and $B_0 = B/(\gamma {h_0}^8)$. We used A_0 = 0.2, B_0 = 2×10^{-6}, and for example, if γ~1 N/m, h_0~1 nm, then the Hamaker constant is *A* ~ 10^{-19}-10^{-18} J, which is comparable to the values reported by Wu, et al.[25] We combined Eq. 2 with the lubrication approximation of the Navier-Stokes equation[26] to derive a governing equation for film thickness evolution, the details of which are in the Supplementary Information.

Using this framework, we investigated the influence of substrate geometry (*i.e.*, pore size, spacing) and initial film thickness (Figure 5). We first designed the nominal mesh template (with a mean pore size of 25 nm spaced by 50 nm) and defined the film thickness, and normalized all other parameters. In the

Nanoscale Accepted Manuscript

simulation output, dewetting is spontaneous, and then proceeds to a quasi-equilibrium state of slow coarsening, at which we calculate the particle order.

The limiting control cases from the simulation are a perfect mesh template and a perfectly flat substrate. We simulate that a perfect mesh template indeed yields a perfectly ordered particle array (Figure S3), and from this perfect case, we can introduce disorder in our simulated template by varying the pore size and spacing according to Gaussian distributions. We show in Figure 5a that particle order decreases nonlinearly with pore order, where ordered arrays resulting only when the pores are highly ordered. For instance, the particle order drops by as much as 42-81% (depending on initial film thickness) when the pore order decreases by only 20%. Furthermore, all of the thickness curves tested converge to the approximate particle order of 0.15 as pore order nears zero, which is nearly the value we calculate for a flat substrate without pores (0.09, Figure S2). This asymptotic behavior represents a lower bound to the disorder of templated particles. Two particles cannot occupy the same volume; they will either coalesce or remain separated by a distance equal to their combined radii. Therefore, an array of 100% uncorrelated particles with order parameter equal to zero is prohibited because it would require particles to overlap in space.

The simulation results corroborate our experimental finding (Figure 4) that templated particles are relatively uncorrelated over large areas but well ordered for small areas, as dictated by the high local ordering of the AAO pores. To demonstrate this, we calculated the values of the pore order and particle order for the AFM images shown in Figure 4 and superimposed them on the plot in Figure 5a. Absolute values between experiment and simulation differ, in part because the simulation uses generalized materials parameters, yet the overall trends are consistent. The simulated image in Figure 5c represents a disordered array of particles that resulted from a mesh with poorly ordered pores, which is corroborated by the lack of order in the inset FFT. The associated histogram in Figure 5b shows that the sizes of the particles (measured by height from the substrate) are large and polydisperse compared to those found in highly ordered arrays.

Particle order is less drastically influenced by variations in pore size (Figure 5d), which we quantified using the standard deviation of normally distributed pore sizes (expressed as a percentage of the pore diameter). Except for large initial film thickness, the particle array remains well-ordered even for large

Nanoscale Accepted Manuscript

pore size variations. For the film thicknesses tested, the order parameter of particle arrays decreases by only 26-42% (greater for larger film thickness) when we vary the pore size by 20%. When the pore size variation is large, the area of each node point varies significantly, which can alter the dewetting and coarsening mechanics. For example, a large area between smaller-than-average pores allows more coarsening via diffusion between adjacent nodes, resulting in agglomeration into larger particles at these locations. Such coarsening is represented in Figure 5f, where the simulated image shows larger particles that grew during dewetting at the expense of adjacent particles, and the accompanying histogram illustrates a bimodal particle size distribution. At the other limit, when the pore order is high and the pore size variation is low (Figure 5e), the resulting particles are highly ordered as well as small and monodisperse compared to other cases tested. To compare with experimental results, we refer back to GISAXS data in Figure 3f, showing that templated Fe particles are small and have a narrow size distribution, as evidenced by the form factor scattering at $q = 0.4\ nm^{-1}$ (as compared to particles on flat alumina without pores, which produce a diffuse form factor centered around $0.7\ nm^{-1}$).

Our results provide insight into the relationship between film thickness and template geometry and how this relationship might scale. In general, we observed in our simulations that particle order increased with decreasing thickness of the initial self-patterned film, with the thinnest film that we tested being approximately equivalent to 0.1-0.2 times the mean pore spacing. Simulations of thick films showed that even for small deviations in pore order (2%), the decay in particle order was substantial (> 60%), which corroborates AFM results for 5-nm-thick films in Figure 3c that exhibited no influence of the underlying mesh substrate. Our AFM analysis also suggested that there is a practical lower limit to the effect of film thickness because if the initial film is too thin, the coverage of particles is compromised, due to overall limited supply of metal atoms to the particles on the substrate surface during dewetting and coarsening. For large AAO pore size and spacing the available top surface area between pores is large, so thin films will not be affected by the porous structure and will dewet randomly as shown in our control cases (Figure 3e and Figure S3). We also note that templated dewetting experiments can be much faster in light of our previous *in situ* SAXS studies that show dewetting is nearly instantaneous. This would mitigate issues that arise due to excessive particle coarsening as well as make for rapid manufacturing.

Nanoscale Accepted Manuscript

Conclusion

We showed that self-ordered metal nanoparticle arrays can be fabricated by dewetting Fe thin films, which are self-patterned on well-ordered AAO substrates. AAO-templated particles were smaller, more monodisperse, and had higher local ordering than those formed by the same process on flat, nonporous substrates. The degree of order is inversely related to the thickness of the initial film, and while the variation in pore size influenced the dewetting process, the spatial organization of the pores ultimately governed the order of particle arrays. We demonstrated local hexagonal ordering of particles, yet the long-range order of the particles is ultimately limited by the ability to fabricate large-area, highly ordered mesh templates. Thus, we believe our study highlights an opportunity and a clear motivation for developing alternative substrates having small template features and long-range order. This scalable templated dewetting approach could be applicable to a variety of metallic thin films on ordered nanoporous substrates, which are potentially relevant to manufacturing of novel catalytic membranes and photonic structures.

Acknowledgements

Financial support for the experimental work (E.R.M. and A.J.H.) was provided by the Office of Naval Research (N00014101055), and the computational work (Z.Z. and W.L.) was supported by the National Science Foundation (CMMI-0927634). Lawrence Livermore National Laboratory is operated by Lawrence Livermore National Security, LLC, for the U.S. Department of Energy, National Nuclear Security Administration under Contract DE-AC52-07NA27344. X-ray scattering was performed in the G1 beamline at the Cornell High-Energy Synchrotron Source (CHESS), which is supported by the NSF and NIH-NIGMS under NSF Grant DMR-0936384. AFM and SEM were performed at the University of Michigan Electron Microbeam Analysis Library (EMAL). E.R.M. received support from the Belgian American Education Foundation and LLNL for data analysis and manuscript preparation. The authors thank Erik Polsen, Mostafa Bedewy, and Megan Roberts, for assistance with AFM, GISAXS, and thin film deposition.

Supplementary Information

Nanoscale Accepted Manuscript

Detailed description of methods including annealing experiments, X-ray scattering, calculation of order parameter, and simulations; carbon nanotube growth results; supplementary AFM and simulation data and analysis.

Nanoscale Accepted Manuscript

References

1. J. C. Hulteen and R. P. Vanduyne, *Journal of Vacuum Science & Technology a-Vacuum Surfaces and Films*, 1995, **13**, 1553-1558.
2. M. Park, C. Harrison, P. M. Chaikin, R. A. Register and D. H. Adamson, *Science*, 1997, **276**, 1401-1404.
3. J. Y. Cheng, C. A. Ross, H. I. Smith and E. L. Thomas, *Advanced Materials*, 2006, **18**, 2505-2521.
4. Y. Lu and A. Lal, *Nano Letters*, 2010, **10**, 2197-2201.
5. J. Joo, B. Y. Chow and J. M. Jacobson, *Nano Letters*, 2006, **6**, 2021-2025.
6. T. Ito and S. Okazaki, *Nature*, 2000, **406**, 1027-1031.
7. C. W. Gwyn, R. Stulen, D. Sweeney and D. Attwood, Chicago, Illinois (USA), 1998.
8. H.-J. Tsai and Y.-L. Lee, *Soft Matter*, 2009, **5**, 2962-2970.
9. J. Lian, L. Wang, X. Sun, Q. Yu and R. C. Ewing, *Nano Letters*, 2006, **6**, 1047-1052.
10. J. D. Fowlkes, L. Kondic, J. Diez, Y. Wu and P. D. Rack, *Nano Letters*, 2011, **11**, 2478-2485.
11. C. V. Thompson, *Annual Review of Materials Research*, 2012, **42**, 399-434.
12. D. SROLOVITZ and S. SAFRAN, *Journal of Applied Physics*, 1986, **60**, 255-260.
13. S. Yang, F. Xu, S. Ostendorp, G. Wilde, H. Zhao and Y. Lei, *Advanced Functional Materials*, 2011, **21**, 2446-2455.
14. A. L. Giermann and C. V. Thompson, *Applied Physics Letters*, 2005, **86**, 121903-121903.
15. J. Basu, C. B. Carter, R. Divakar, B. Mukherjee and N. Ravishankar, *Applied Physics Letters*, 2009, **94**, 171114-171113.
16. J. Petersen and S. G. Mayr, *Journal of Applied Physics*, 2008, **103**, 023520-023528.
17. F. Ruffino and M. G. Grimaldi, *Applied Surface Science*, 2013, **270**, 697-706.
18. J. Ye and C. V. Thompson, *Advanced Materials*, 2011, **23**, 1567-1571.
19. P. Farzinpour, A. Sundar, K. D. Gilroy, Z. E. Eskin, R. A. Hughes and S. Neretina, *Nanoscale*, 2013, **5**, 1929-1938.
20. E. R. Meshot, E. Verploegen, M. Bedewy, S. Tawfick, A. R. Woll, K. S. Green, M. Hromalik, L. J. Koerner, H. T. Philipp, M. W. Tate, S. M. Gruner and A. J. Hart, *ACS Nano*, 2012, **6**, 5091-5101.

Nanoscale Accepted Manuscript

21. J. R. Levine, J. B. Cohen, Y. W. Chung and P. Georgopoulos, *Journal of Applied Crystallography*, 1989, **22**, 528-532.
22. H. Gong, W. Lu, L. Wang, G. Li and S. Zhang, *Journal of Applied Physics*, 2012, **112**.
23. W. Lee, R. Ji, U. Gösele and K. Nielsch, *Nat Mater*, 2006, **5**, 741-747.
24. J. Becker, G. Grun, R. Seemann, H. Mantz, K. Jacobs, K. R. Mecke and R. Blossey, *Nat Mater*, 2003, **2**, 59-63.
25. Y. Wu, J. D. Fowlkes, P. D. Rack, J. A. Diez and L. Kondic, *Langmuir*, 2010, **26**, 11972-11979.
26. A. Oron, S. H. Davis and S. G. Bankoff, *Reviews of Modern Physics*, 1997, **69**, 931-980.

Nanoscale Accepted Manuscript

311 **Figures**

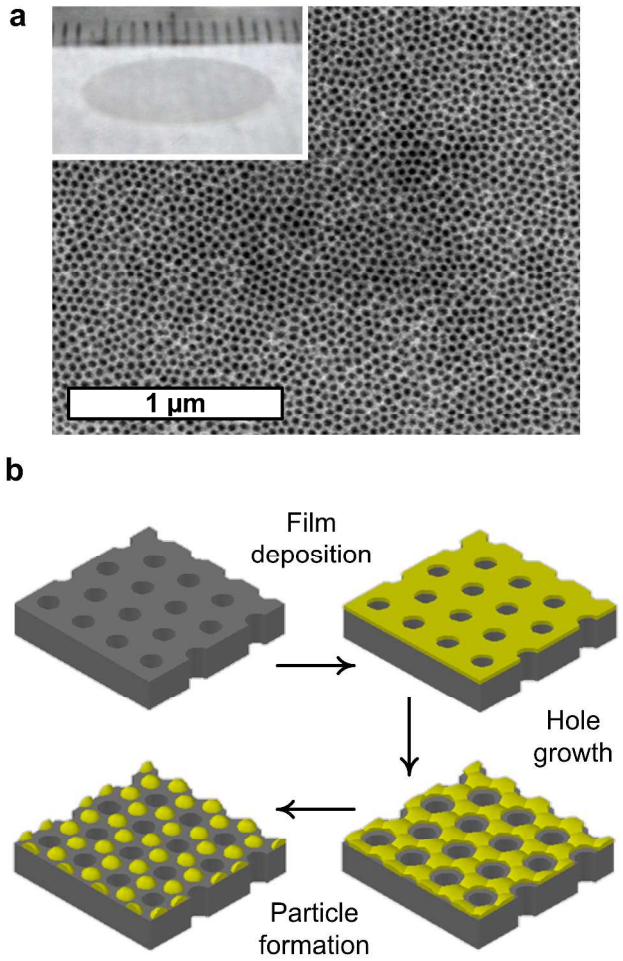

312

313

314 Figure 1. Process of templated dewetting on AAO templates. (a) SEM of the top surface with inset
315 photograph of AAO templates used in this study (reported mean pore diameter is 18 nm; Synkera, Inc.).
316 The ruler marks in the photograph represent millimeters. (b) Preparation of AAO-supported metal
317 nanoparticles by sputter deposition of a thin film followed by thermal annealing. According to classical
318 detwetting theory, dewetting of the film is driven by surface tension whereby holes in the film grow until
319 islands pinch off, ideally leaving individual particles at the node points of the AAO template.

320

Nanoscale Accepted Manuscript

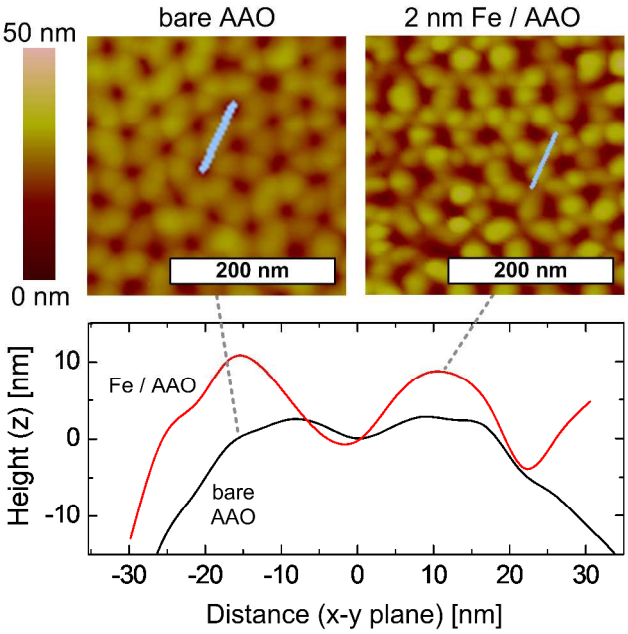

Figure 2. AFM analysis of topographical comparison between bare AAO and ordered Fe particles after annealing/dewetting of 2 nm Fe on AAO. The traces shown in the spline plot are taken from respective AFM images as indicated by the light blue lines. The origin of the plot was selected to be at the center of a node point. AAO substrates had 18-nm pore size and 49-nm pore spacing.

Nanoscale Accepted Manuscript

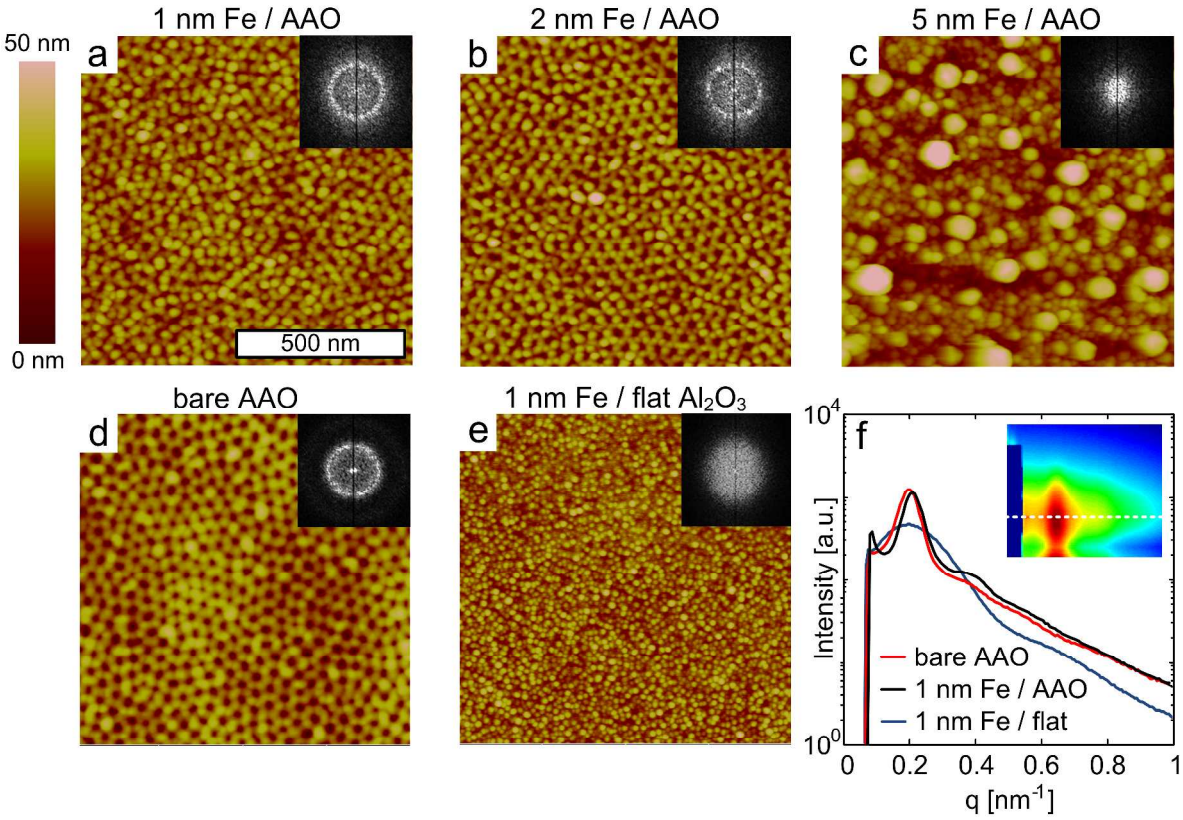

Figure 3. Study of Fe film thickness order and monodispersity of templated nanoparticles. AFM images (with inset corresponding FFT) comparing the surface morphology after thermal annealing of (a) 1 nm Fe on AAO, (b) 2 nm Fe on AAO, (c) 5 nm Fe on AAO as well as (d) bare AAO and (e) 1 nm Fe on flat Al_2O_3. (f) GISAXS of samples shown in (a), (d), and (e). AAO substrates had 18-nm pore size and 49-nm pore spacing.

Nanoscale Accepted Manuscript

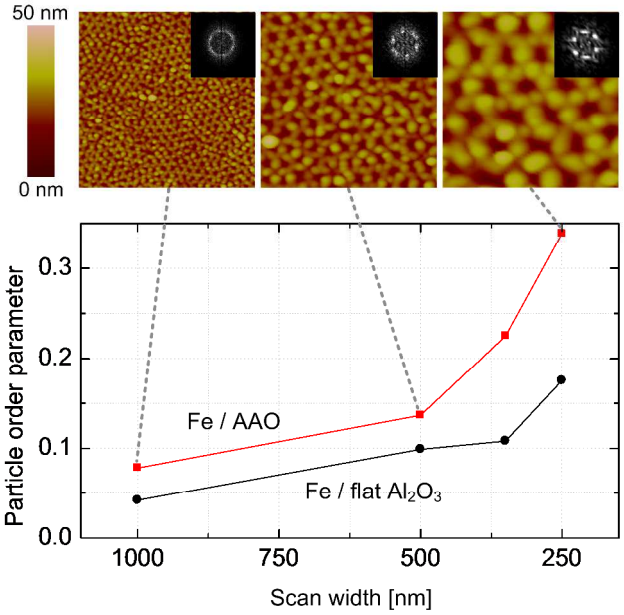

Figure 4. Influence of AAO template on short- and long-range order of Fe particle arrays after annealing. Scan size was established by selecting subsequently smaller areas on an AFM image of 2 nm Fe on AAO (shown above plot) and 1 nm Fe on flat Al_2O_3 (not shown). AAO substrates had 18-nm pore size and 49-nm pore spacing.

Nanoscale Accepted Manuscript

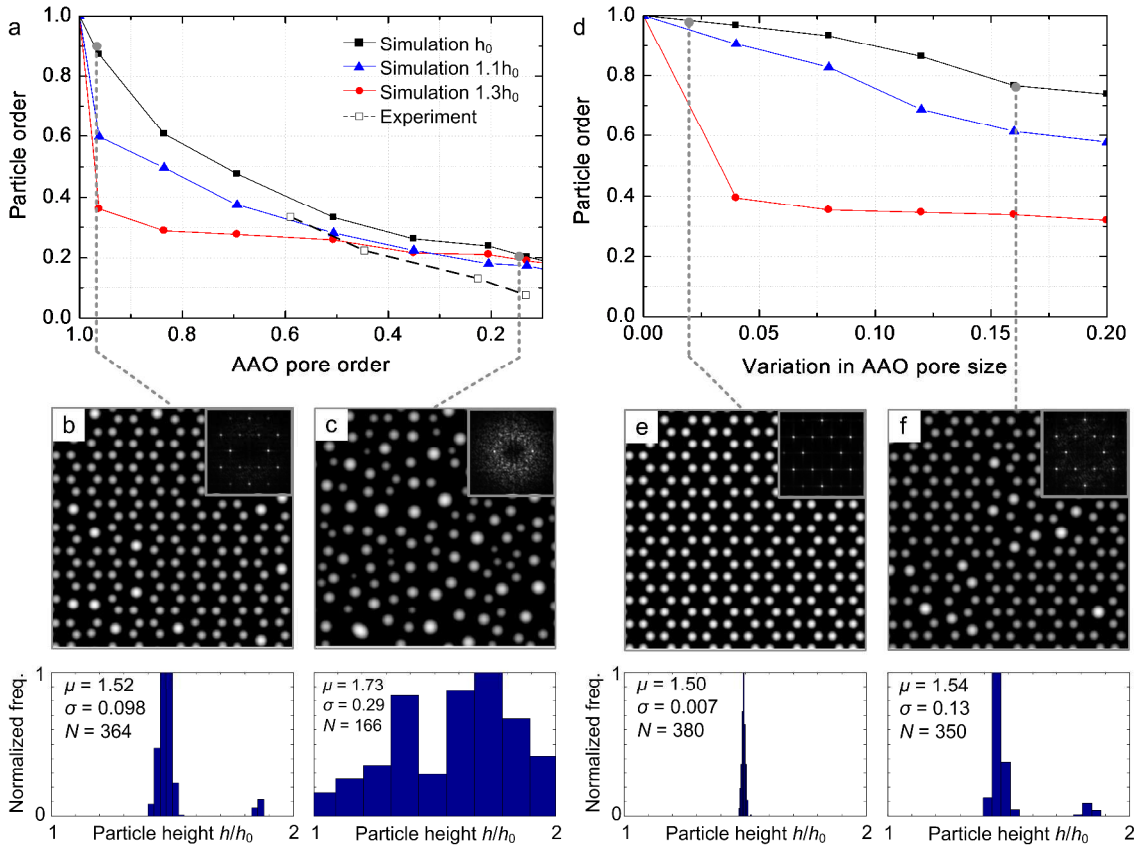

Figure 5. Simulation study of how the particle order is influenced by both the order of the AAO substrate and the variation in AAO pore size. Order parameters calculated from AFM images (from Figure 4) are shown (black hollow square, dashed line) in a) for comparison. Image and inset FFT are shown for several representative simulation conditions, illustrating relative changes in order and polydispersity, where (e) represents nearly perfect order and monodispersity. Simulations were performed with a mean pore size of 25 nm spaced by 50 nm, and data are normalized to h_0, where images are 500 x 500 and accompanying histograms tabulate the measured height of each particle.

Nanoscale Accepted Manuscript